Generating spin squeezing states and Greenberger-Horne-Zeilinger entanglement using a hybrid phonon-spin ensemble in diamond

Keyu Xia (夏可宇)* and Jason Twamley
ARC Centre for Engineered Quantum Systems, Department of Physics and Astronomy, Macquarie University, New South Wales 2109, Australia

(Received 5 May 2016; revised manuscript received 1 October 2016; published 10 November 2016)

Quantum squeezing and entanglement of spins can be used to improve the sensitivity in quantum metrology. Here we propose a scheme to create collective coupling of an ensemble of spins to a mechanical vibrational mode actuated by an external magnetic field. We find an evolution time where the mechanical motion decouples from the spins, and the accumulated geometric phase yields a squeezing of 5.9 dB for 20 spins. We also show the creation of a Greenberger-Horne-Zeilinger spin state for 20 spins with a fidelity of ∼0.62 at cryogenic temperature. The numerical simulations show that the geometric-phase-based scheme is mostly immune to thermal mechanical noise.

DOI: 10.1103/PhysRevB.94.205118

I. INTRODUCTION

Electronic spins associated with nitrogen-vacancy (NV) centers in diamond possess ultralong coherent times in their ground states at room temperature [1,2], and can be initialized, controlled, and read out using magnetic and optical fields. These features motivate intensive interest in NV-based quantum information processing [3] and sensing applications. For instance the NV center has been used for quantum computing [4,5], cavity quantum electrodynamics systems [6], hybrid quantum interfaces [7], nanoscale magnetometry [8–10], ultrahighly precise solid magnetometry [11–13], thermometers [14–16], and nanoscale imaging [17,18].

The application of the squeezed spin state (SSS) and the Greenberger-Horne-Zeilinger (GHZ) spin state can boost the precision of quantum metrology [19]. Spin squeezing has been typically realized in atomic ensembles [20–23], while the state-of-the-art experiment has achieved 20 dB squeezing using half a million ultracold Rb atoms in a natural atomic trap [21]. It is of interest to squeeze solid-state spins as this can lead to potentially novel sensor applications. The NV center has a solid-state spin-1 triplet ground state. The squeezing of NV centers has been proposed with the help of the strain-induced spin-phonon Tavis-Cummings type interaction [24]; however, small amounts of thermal excitation can completely inhibit the squeezing. The standard quantum limit in quantum metrology can also be surpassed by using an entangled GHZ state. To date, entangled Bell's states and small GHZ states [25–27] have been generated in various systems, but a GHZ spin state with more than 10 spins has yet to be demonstrated in the literature.

In this paper we describe an approach to engineer the collective coupling of an ensemble of NV centers to a mechanical resonator, mediated by an external magnetic field. Using our protocol, at time $t_m = 2m\pi/\omega_m$, where ω_m is the mechanical oscillation frequency and m is an integer, the mechanical resonator decouples from the NV spin ensemble. We find that the accumulated geometric phase on the NV centers can create a SSS of up to 20 spins whose squeezing is ∼5.9 dB at a large m. We also find that our protocol can generate with high fidelity a GHZ state of up to 20 electronic spins. This paper provides a precise numerical investigation of the influence of thermal mechanical noise on the squeezing and the fidelity of the achieved GHZ spin state. In contrast to Bennett's work [24], our geometric-phase-based scheme is robust against thermal mechanical noise. We note that Zhang *et al.* very recently analytically studied the squeezing of 10 NV centers coupling to mechanical motion [28]. However, our method is more accurate and can provide a useful prediction for larger spin ensembles. Moreover, in contrast to previous work [28] exploring the trapped nanodiamond, our scheme for spin squeezing and entanglement uses a diamond nanowire. We also discuss the generation of GHZ states.

II. SYSTEM AND MODEL

The schematic setup for squeezing and entanglement of an ensemble of NV spin centers in a nanodiamond is depicted in Fig. 1(a).

In the setup a nanodiamond oscillates along the x axis with a mechanical frequency ω_m corresponding to an oscillation period of $T_m = 2\pi/\omega_m$. The nanodiamond can be a part of a micro/nanocantilever [29], or attached to a nanotube [30]. Alternatively, the nanodiamond can be optically trapped in near vacuum [31,32]. Instead, we choose a single-crystal diamond nanowire with a diameter d and length L for the mechanical resonator [33–36].

We assume the mass of the entire mechanical resonator to be m, yielding a zero-point fluctuation of $x_{\rm zp} = \sqrt{\hbar/2m\omega_m}$ and a mechanical quality factor of Q_m corresponding to a delay rate of $\gamma_m = \omega_m/Q_m$. The mechanical motion can be quantized as $x = x_{\rm zp}(b^\dagger + b)$, where $b^\dagger$ and b are the creator and annihilation operators of mechanical oscillation. At temperature T, the mechanical decoherence due to the thermal excitation is $\bar{n}\gamma_m$ with $\bar{n} = [e^{\hbar\omega_m/k_BT} - 1]^{-1}$, where k_B is the Boltzman constant. Recent experiments [29] have demonstrated various diamond micro/nanomechanical resonators with frequencies ranging from 2 kHz to several MHz and with quality factors Q_m up to $\sim 10^7$. The quality factor Q_m of a diamond nanowire can also surpass 10^6 [33], but the resonance frequency is

*keyu.xia@mq.edu.au

 ©2016 American Physical Society

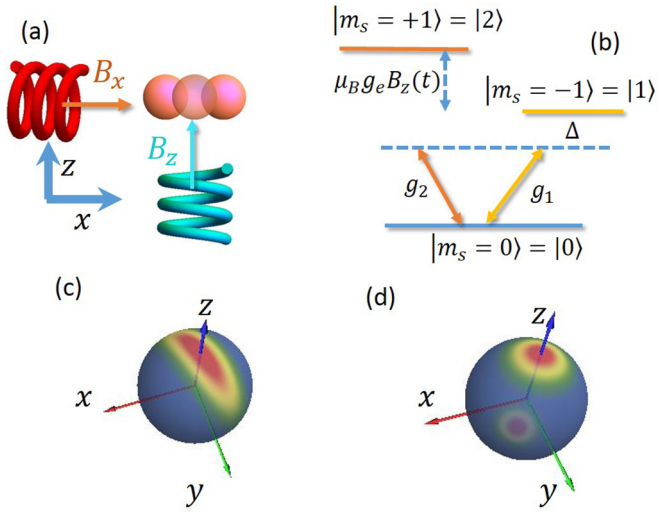

FIG. 1. Schematic diagrams for system squeezing and entangling an ensemble of electron spins in a nanodiamond. (a) An ensemble of NV centers in a nanodiamond oscillates along the x direction with a resonance frequency ω_m. The principal axis of the nanodiamond is cut along the z direction. A magnetic field B_z is parallel to the z axis, while the magnetic field $B_x(x)$ is applied along the x direction and has a giant gradient along the x direction. (b) A level diagram of the NV centers in a nanodiamond. (c) The Bloch sphere representation of squeezed $N = 20$ NV centers. (d) The Bloch sphere representation of the GHZ state of $N = 20$ NV centers.

higher. These high-Q nanomechanical resonators allow us to obtain the required geometric phase with a reasonable magnetic gradient. To make a spin-mechanical hybrid system we can embed NV centers in the end of the diamond nanowire.

We use a magnetic field $\mathbf{B} = B_x(x)\hat{x} + B_z\hat{z}$ to engineer the quantum coupling between the ground states of the NV centers and the mechanical motion, where $\hat{x}(\hat{z})$ is the unit vector along the $x(z)$ direction. Each NV center has a triplet ground state with levels $|m_s = 0,\pm 1\rangle$, as shown in Fig. 1(b). The Hamiltonian of the ground states of the jth NV center in the magnetic field can be described by ($\hbar = 1$)

$$H_j = D_j S_{z,j}^2 + \gamma_B \mathbf{S}\cdot\mathbf{B}, \tag{1}$$

where $D_j \approx 2\pi \times 2.87$ GHz [37,38], $\gamma_B \approx 2\pi \times 28$ GHz/T is the gyromagnetic ratio of electron, and $\mathbf{S}$ the electron spin operator.

The homogeneous magnetic field component B_z shifts the state $|m_s = -1\rangle = |1\rangle(|m_s = +1\rangle = |2\rangle)$ down (up) by $\gamma_B B_z$, while $|m_s = 0\rangle = |0\rangle$ is unshifted, as shown in Fig. 1(b).

Here we neglect the hyperfine interaction of which the coupling strengths are typically few MHz [39,40]. This is reasonable because the nuclear spins can be polarized to a selective nuclear spin state and only allow one hyperfine transition [41–43].

We consider the magnetic field $\mathbf{B}$ to possess a giant gradient $G_B = \frac{\partial B_x(x)}{\partial x}$ along the x direction. We engineer this field so that $B_x(x_0) = 0$ at the equilibrium position $x_0 = 0$ of the mechanical resonator. We expand the Hamiltonian in Eq. (1) to the first order of the magnetic field gradient such that

$$H_j = D_j S_{z,j}^2 + \gamma_B B_z(|2\rangle_j\langle 2| - |1\rangle_j\langle 1|) + (b^\dagger + b)\big[g_1^{(j)}|1\rangle_j\langle 0| + g_2^{(j)}|2\rangle_j\langle 0| + \text{H.c.}\big], \tag{2}$$

where $g_1^{(j)}(g_2^{(j)})$ is the magnetic coupling to the transition $|1\rangle(|2\rangle) \leftrightarrow |0\rangle$ of the jth spin. In this arrangement the interaction between the mechanical motion and the NV spin ensemble mediated by the magnetic field gradient G_B can be described by the interaction Hamiltonian

$$H_I^{(x)} = \sum_j (b^\dagger + b)\big[g_1^{(j)}|1\rangle_j\langle 0| + g_2^{(j)}|2\rangle_j\langle 0| + \text{H.c.}\big]. \tag{3}$$

For simplicity, we assume identical coupling such that $g_x = g_1^{(j)} = g_2^{(j)} = \gamma_B G_B x_{\text{zp}}$. Taking $B_z \sim 0.1$T, the frequency $\omega_j = D_j - \gamma_B B_z$ indicating the energy gap between the ground states $|m_s = -1\rangle(|1\rangle)$ and $|m_s = 0\rangle$ is vanishing small but that between $|m_s = 1\rangle(|2\rangle)$ and $|m_s = 0\rangle$ can be about $2\pi \times 5.6$ GHz. Here we neglect the inhomogeneous broadening in D_j because it is about 1kHz, much smaller than the mechanical vibration frequency [1,2]. For the purpose of squeezing and entanglement, at $B_z = 0.1$T, we can neglect the coupling to the transition between $|2\rangle$ and $|0\rangle$ due to the high energy gap. After dropping the state $|2\rangle$, the Hamiltonian describing the dynamics of the system reduces to

$$H_x = \sum_j \omega_j |1\rangle_j\langle 1| + \omega_m b^\dagger b + \sum_j g_x(b^\dagger + b)(|1\rangle_j\langle 0| + |0\rangle_j\langle 1|). \tag{4}$$

We set $\omega_j = \omega_0$ and $\Delta = \omega_0 - \omega_m$. We define collective spin operator $J_z = \sum_j(|m_s = -1\rangle_j\langle m_s = -1| - |m_s = 0\rangle_j\langle m_s = 0|)/2$, $J_+ = \sum_j |m_s = -1\rangle_j\langle m_s = 0|$, and $J_- = \sum_j |m_s = 0\rangle_j\langle m_s = -1|$ to obtain

$$H_x = \omega_0(J_z + \mathcal{I}/2) + 2g_x(b^\dagger + b)J_x + \omega_m b^\dagger b, \tag{5}$$

with $\mathcal{I} = \sum_j(|m_s = -1\rangle_j\langle m_s = -1| + |m_s = 0\rangle_j\langle m_s = 0|)$ and $J_x = (J_+ + J_-)/2$. We now neglect the term $\omega_0\mathcal{I}/2$ as it only yields a geometric phase in the evolution. To accommodate the extensively large Hilbert space spanned by a large ensemble of NV centers we apply the Holstein-Primakoff (HP) transformation [44,45], yielding $J_z = (a^\dagger a - \frac{\mathcal{N}}{2})$, $J_+ = a^\dagger\sqrt{\mathcal{N} - a^\dagger a}$, and $J_- = \sqrt{\mathcal{N} - a^\dagger a}a$ with $\mathcal{N} = N\mathcal{I}$. In the HP picture the Hamiltonian H_x in Eq. (5) becomes

$$H_{\text{HP}} = \omega_0 a^\dagger a + \lambda(b^\dagger + b)\bar{J}_x + \omega_m b^\dagger b, \tag{6}$$

where $\lambda = 2\sqrt{N}g_x$ and $\bar{J}_x = (a^\dagger\sqrt{\mathcal{I} - a^\dagger a/N} + \sqrt{\mathcal{I} - a^\dagger a/N}a)/2$ is the Dicke-model collective spin operator. In the limit $N \to \infty$ and $\langle a^\dagger a\rangle/N \ll 1$, the Hamiltonian H_{HP} reduces to

$$H_{\text{Dicke}} = \omega_0 a^\dagger a + \frac{\lambda}{2}(b^\dagger + b)(a^\dagger + a) + \omega_m b^\dagger b. \tag{7}$$

If we set the magnetic field component $B_z = 0.1$T so that one works at the level crossing $\omega_0 = 0$, the Hamiltonian in the interaction picture of $\omega_m b^\dagger b$ becomes

$$V_x = \lambda(b^\dagger e^{i\delta t} + be^{-i\delta t})\bar{J}_x, \tag{8}$$

with $\delta = \omega_m$. By applying the Magnus formula [46], the dynamics for the system can be described exactly, in the absence of decoherence, by the unitary evolution operator

$$U_x(t) = e^{iN\theta(t)\bar{J}_x^2} e^{\lambda/\delta[\alpha(t)b^\dagger - \alpha^*(t)b]\bar{J}_x}, \tag{9}$$

with $\alpha(t) = 1 - e^{i\delta t}$ and $\theta(t) = (\frac{2g_x}{\delta})^2(\delta t - \sin\delta t)$. $\theta(t)$ is the unconventional geometric phase which depends only on the global geometric features of operators and is robust again random operation errors [47]. $\alpha(t)$ is a periodic function modulating the spin-mechanical coupling. At $t_m = 2m\pi/\delta$ for an integer m, $\alpha(t)$ vanishes, $\theta(t_m) = 2m\pi(\frac{2g_x}{\delta})^2$, and the mechanical motion decouples from the NV centers. As a result, the evolution operator for the spin ensemble can be explicitly expressed as

$$U_x(t_m) = e^{iN\theta(t_m)\bar{J}_x^2}. \tag{10}$$

Starting from an initial state $|\psi_0\rangle$ the generated state at t_m is $|\psi(t_m)\rangle = U_x(t_m)|\psi_0\rangle$. Note that the squeezing degree of the SSS is only dependent on the available $\theta(t_m)$, which can be controlled with the coupling rate g_x as normal and the number of mechanical period m.

Below we will use this evolution operator to squeeze an ensemble of electronic spins for a small $\theta(t_m) = 2m\pi(\frac{2g_x}{\delta})^2$; see Fig. 1(c). The scheme can also generate the GHZ state of $N \sim 20$ electron spins if $\theta(t_m) = \pi/2$ is obtainable; see Fig. 1(d) [48,49]. In contrast to the previous scheme using a Tavis-Cummings type strain-spin interaction in the dispersive regime [24], whose coupling results from a small phononic ac Stark shift, our scheme is superior since the coupling strength is not suppressed by a large detuning. Importantly, our geometric-phase-based scheme is immune to many types of noise such as dephasing noise and to first order of spin relaxation since it squeezes the spins via geometric phase control which is known to be quite robust to noise [47]. Moreover, the coupling strength λ can be tuned by engineering the gradient of the magnetic field. Throughout the further investigation, we will focus on the first cycle of mechanical vibration, i.e., $m = 1$ in t_m. Later on, we will discuss the operation at a larger integer m requiring a longer evolution time. If the decoherence of the NV centers and the mechanical resonator is small enough, then a large number $m > 1$ is preferable because a smaller magnetic field gradient and a larger size of the mechanical resonator are applicable.

The explicit evolution operator in Eq. (10) can provide an apparent picture for understanding the unitary evolution of the system. It shows that the initial thermal mechanical occupation is decoupled from spins at $t_1 = 2\pi/\omega_m$. Here, we set $m = 1$ for using the first cycle of mechanical vibration. However it is difficult to include the effect of the mechanical relaxation. The effect may be considerable in some cases due to thermal excitation of the mechanical motion. To consider the mechanical relaxation, we numerically study the evolution of the combined system by solving the quantum Langevin equation in the bosonic picture after the Holstein-Primakoff transformation

$$\begin{aligned}\partial\rho/\partial t = &-i[H_{\rm HP},\rho] + \mathscr{L}\{(\bar{n}+1)\gamma_m, b, \rho\} \\ &+\mathscr{L}\{\bar{n}\gamma_m, b^\dagger, \rho\},\end{aligned} \tag{11}$$

where $\mathscr{L}\{\gamma, A, \rho\} = \gamma/2\{2A\rho A^\dagger - A^\dagger A\rho - \rho A^\dagger A\}$ for $\gamma \in \{\bar{n}\gamma_m, (\bar{n}+1)\gamma_m\}$ and $A \in \{b, b^\dagger\}$. Recent experiments have demonstrated ultralong coherence times $T_2 \sim 1$ms in ensembles of electron spins in diamond even at room temperature [1,2]. The relaxation time T_1 of the NV spin ensemble has also been reported to be much longer, up to several minutes at low temperature [50]. Obviously, both T_1 and T_2 are much longer than our operation time. Moreover, our geometric-phase-based scheme is robust again dephasing [47], so we ignore the decoherence of the spin ensemble in the quantum Langevin equation. The noise is dominated by the mechanical thermal noise. As long as $m\bar{n}\gamma_m/\omega_m \ll 1$, we will achieve a highly squeezed spin state and a high-fidelity GHZ state.

In the case where the inhomogeneity of the couplings and the transition frequencies ω_j are negligible, dark states are rarely excited. The state of the system can be fully described by the Dicke model defined in Eqs. (10) and (11). The Dicke state $|J,m\rangle$ with $m \in \{-J, -J+1, \ldots, J+1, J\}$ in the spin picture is equivalent to the Fock state $|J+m\rangle$ in the bosonic picture [19]. Thus, a GHZ state of spin, $|\mathrm{GHZ_{spin}}\rangle = (|0\rangle^{\otimes N} + |1\rangle^{\otimes N})/\sqrt{2}$, corresponds to the cat state $|\mathrm{GHZ_a}\rangle = (|0\rangle + |N\rangle)/\sqrt{2}$ in the bosonic picture.

In the bosonic picture, the squeezing degree of spin states $\{|0\rangle, |1\rangle\}$ of NV centers can be evaluated by the squeezing parameter ξ_s^2 given by Kitagawa and Ueda as [19] $\xi_s^2 = 1 + 2\langle a^\dagger a\rangle - \frac{2\langle (a^\dagger a)^2\rangle}{N} - 2|\langle \bar{J}_x^2\rangle|$. Correspondingly, the squeezing parameter defined by Wineland *et al.* is related to ξ_s^2 via $\xi_R^2 = (\frac{N}{2|\langle \vec{J}\rangle|})^2\xi_s^2$ with $|\langle \vec{J}\rangle| = \sqrt{\langle J_x\rangle^2 + \langle J_y\rangle^2 + \langle J_z\rangle^2}$ [19], while the fidelity of generated GHZ state can be directly calculated as $F = \mathrm{Tr}[\rho|\mathrm{GHZ_a}\rangle\langle\mathrm{GHZ_a}|]$ [19].

Before preparation of the squeezing and GHZ states we first optically polarize the NV centers to their ground states $|m_s = 0\rangle$. Then we apply $B_z = 0.1$T to bring $\omega_0 = 0$. Since then, the system begins to evolve under the Hamiltonian Eq. (6).

III. RESULTS

A. Preparation of squeezing spin states

Without noise from mechanical motion, the squeezing of the NV spin ensemble is maximal when θ is the so-called optimal phase $\theta_{\rm opt} = 6^{-1/6}(N/2)^{-2/3}$ (see Appendix). The corresponding squeezing parameter defined by Kitagawa and Ueda is $\xi^2_{\rm opt} = N^{-2/3}$ [19]. $\theta_{\rm opt}$ can be very small for a large number of NV$^-$s. Noting that $\theta = (\frac{2g_x}{\omega_m})^2\omega_m t_m$, we find that the coupling g_x can be quite small in order to squeeze a large ensemble of spins. For a large integer m, g_x can be further reduced by a factor of $\sqrt{m}$. This allows the squeezing of an ensemble of spins even for a relatively small spin-phonon coupling. A nanomechanical resonator with small mass but high quality factor is preferable because it promises a large coupling under a relatively small magnetic gradient and small noise. For our general numerical investigations we choose $Q_m = 10^6$ for our mechanical resonator [29]. We first investigate the target state at the time $t_1 = 2\pi/\omega_m$ when the mechanical motion and the spins separate. Then we will look into the target state at a large m which allows a small coupling rate g_x to achieve the optimal phase. The phase θ can be

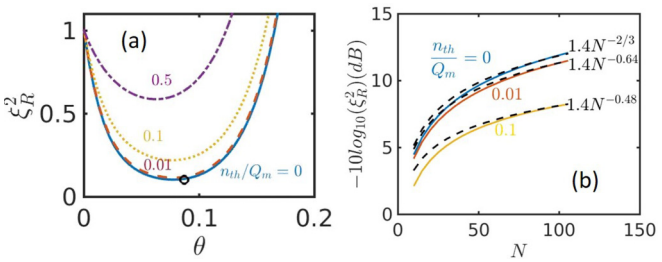

FIG. 2. (a) Squeezing parameter ξ_R^2 for $N = 50$ spins as a function of θ for different thermal noise $\bar{n}/Q_m$. (b) Optimal squeezing parameter ξ_R^2 (dB) as a function of number of spins, N at different thermal noises $\bar{n}/Q_m = 0,0.01,0.1$. The numerical results are fitted by $1.4N^{-2/3}$,$1.4N^{-0.64}$, and $1.4N^{-0.48}$.

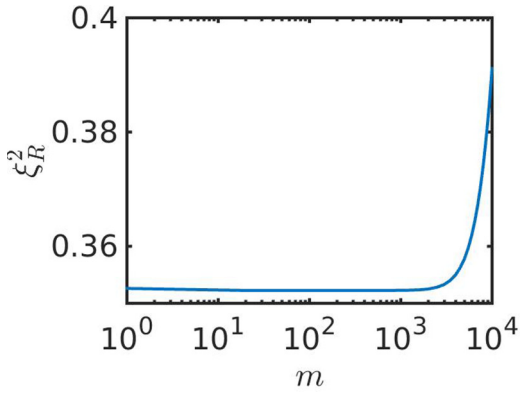

FIG. 3. Squeezing parameter ξ_R^2 for $N = 10$ spins at different m but fixed $\theta(t_m)$. Here $Q_m = 10^6$,$\bar{n} = 10$.

adjusted at the fixed time t_m by controlling the gradient of the magnetic field.

Now we investigate the attainable squeezing by numerically solving the master equation taking into account the mechanical thermal noise. First, we study the effect of mechanical noise on the squeezing parameter ξ_R^2 at the optimal phase $\theta_{\text{opt}} = 0.087$ rad at fixed time t_1 for $N = 50$ spins; see Fig. 2(a). This optimal phase requires $g_x/2\pi = 29.4$ kHz for $N = 50$ NV centers. Such coupling strength is obtainable in a nanomechanical resonator system [51,52]. As can be seen in Fig. 2(a), the squeezing parameter first decreases as the phase θ (or the coupling g_x) increases. After reaching the maximal squeezing, it increases as θ continues to increase. At a low temperature $\bar{n}/Q_m = \bar{n}\gamma_m/\omega_m \leqslant 0.01$ corresponding to $\bar{n} = 10^4$, our scheme can achieve the optimal squeezing $\xi_s^2 = N^{-2/3}$ and $\xi_R^2 = 1.4N^{-2/3}$ at θ_{opt}, as shown by the black circle. Even for $\bar{n}/Q_m = 0.1$, ξ_R^2 (ξ_s^2) only increases to 0.23 (0.15) from 0.1 (0.074) for $\bar{n}/Q_m = 0$. Moreover, the optimal phase decreases very slightly with order variations in $\bar{n}/Q_m$, indicating robust squeezing against mechanical thermal noise. This is an important advantage of this geometric-phase-based squeezing scheme. Even at $\bar{n}/Q_m = 0.5$ we are still able to squeeze the spins by $\xi_R^2 \sim 1.67$ dB.

By numerically solving the master equation for N up to 105 we study the dependence of the squeezing on the spin number and the thermal noise. Then we provide an estimate of achievable squeezing for a large ensemble of spins, as shown in Fig. 2(b). We calculate the squeezing ξ_R^2 for different N at the phase $\theta = \theta_{\text{opt}}$. When $\bar{n} = 0$, the ideal squeezing is $\xi_R^2 = 1.4N^{-2/3}$, as shown by the blue line and its fitting. The available squeezing slightly reduces to $\xi_R^2 = 1.4N^{-0.64}$ when the thermal noise dramatically increases to $\bar{n}/Q_m = 0.01$, and can still reach $1.4N^{-0.48}$ when the thermal noise reaches $\bar{n}/Q_m = 0.1$. Remarkably, the phase uncertainty in measurement, $\Delta\phi = \xi_R/\sqrt{N}$, can be reduced as the number of spins increases. Note that such squeezing degree of many spins is crucially dependent on the available large gradient G_B of the magnetic field.

As mentioned above, applying a large integer m can relax the required magnetic gradient. As long as $m\bar{n}/Q_m \ll 1$, we can obtain mostly the optimal squeezing. As shown in Fig. 3 as an example for $N = 10$ spins, the squeezing is close to the optimal squeezing $\xi_R^2 = 0.35$ when $m < 2 \times 10^3$. Even when m increases to 10^4, we still have $\xi_R^2 < 0.4$ corresponding to 4 dB squeezing.

B. Preparation of GHZ states

In contrast to squeezing only requiring small θ, the generation of the GHZ state requires $\theta = \pi/2$ which requires a large coupling strength g_x.

We first compare the fidelity of the numerically evaluated GHZ state for $N = 10$ and $N = 20$ NV centers under mechanical thermal noise; see Fig. 4(a). When the number of spins is doubled, the fidelity as a function of $\bar{n}/Q_m$ shifts to the left slightly. In both cases the fidelity can be larger than 0.95 if $\bar{n}/Q_m < 10^{-3}$ is available. The fidelity is still higher than 0.5 as $\bar{n}/Q_m$ decreases to 0.03 or 0.05 for 20 or 10 spins, respectively. Figure 4(b) shows the limit of the mechanical thermal noise to achieve a fidelity of $F = 0.5$ and 0.9 for different numbers of spins. It can be clearly seen that we can prepare the GHZ state with a fidelity of $F = 0.9$ for

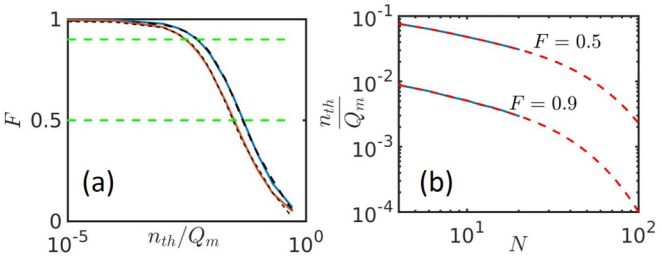

FIG. 4. (a) Fidelity of the generated GHZ state as a function of thermal noise, $\bar{n}/Q_m$, for $N = 10$ (blue line) and $N = 20$ (red line) fitted two-term exponential functions, $ae^{b\bar{n}/Q_m} + ce^{d\bar{n}/Q_m}$, with $\{a = 0.5208,b = -32.58,c = 0.4722,d = -4.241\}$ (dashed black lines) and $\{a = 0.5182,b = -54.21,c = 0.4704,d = -6.016\}$ (dotted-dashed black lines), respectively. Green lines are guide to eyes at $F = 0.5,0.9$. (b) The mechanical thermal decoherence limit for achieving the set fidelity ($F = 0.5,0.9$) for different number of NV$^-$s. Blue lines are numerical results by solving the master equation. Dashed red lines are the two-term exponential fitting by $ae^{bN} + ce^{dN}$ with $\{a = 0.063,b = -0.229,c = 0.058,d = -0.032\}$ for $F = 0.5$ and $\{a = 9.248^{-3},b = -0.277,c = 6.816^{-3},d = -0.042\}$ for $F = 0.9$.

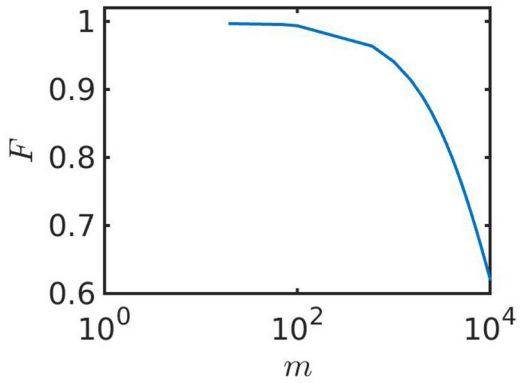

FIG. 5. Fidelity of the GHZ state for $N = 10$ spins at different m but a fixed $\theta = \pi/2$. Here $Q_m = 10^6, \bar{n} = 10$.

up to 20 NV^-s if $\bar{n}/Q_m < 3 \times 10^{-3}$ is possible. The fidelity can still be larger than 0.5 if the thermal noise increases to $\bar{n}/Q_m = 2 \times 10^{-2}$. Note that this geometric phase protocol can generate the GHZ state only for an even number of spins.

As the generation of the SSS, we can create with a high fidelity the GHZ state at a large integer m as well if $m\bar{n}/Q_m \ll 1$ is met. As shown in Fig. 5, increasing m will introduce more noise in the target state and subsequently lead to smaller fidelity. However, the fidelity of the GHZ state can be larger than 0.8 when $m < 4 \times 10^3$, i.e., $m\bar{n}/Q_m < 0.04$.

IV. MAGNETIC FIELD

In this section, we simulate the distribution of the x component of the magnetic field generated by a permanent magnetic tip. We do the two-dimensional simulation with FEMM 4.2. The magnetic field generated by a real three-dimensional magnetic tip is axis symmetrical. We use the material SmCo27MGOe from the material library of FEMM for the magnetic tip. The structure of the tip is shown in Fig. 6(a) (blue box). The tip is 2 μm thick and 3 μm wide. The transversal component of the magnetic field (B_z) is negligible in the region we are interested in. If we use a plane surface for the tip (see the right-hand side of the tip), then the magnetic field in the middle region is weaker than that in edge, and subsequently its transversal distribution is considerably curved. To create a uniform distribution of the field B_x, we design a convex curved surface of which the cross section is a 30° arc connecting the two points, $(-1\ \mu\text{m}, 1.5\ \mu\text{m})$ and $(-1\ \mu\text{m}, -1.5\ \mu\text{m})$. As seen in Figs. 6(b) and 6(d), the transversal distribution of the field B_x is very uniform over about 180 nm. Its fluctuation is much smaller than 0.1 mT. The gradient of the field B_x is uniform over 500 nm as well, and $\partial B_x/\partial x \approx 2.3 \times 10^5$ T/m; see Fig. 6(c). Such design can provide us a practical implementation for our proposal. Through simulation we find that the bigger the diameter of the tip is, the smaller the gradient and the wider the transversal uniform region. If we only require a uniform field over ~50 nm in the transversal section, the available gradient can be much larger.

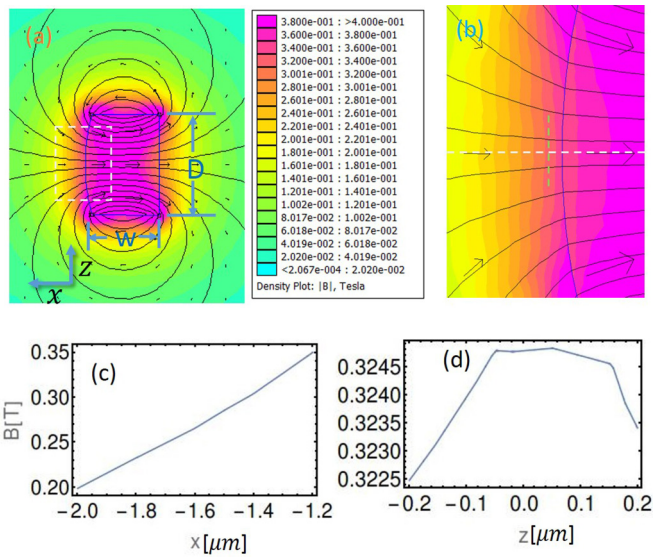

FIG. 6. Magnetic field B_x generated by a two-dimensional permanent magnetic tip made from SmCo27MGOe (simulated with FEMM 4.2). The coordinates of the four points are $\{(-1\ \mu\text{m}, 1.5\ \mu\text{m}), (1\ \mu\text{m}, 1.5\ \mu\text{m}), (1\ \mu\text{m}, -1.5\ \mu\text{m}), (-1\ \mu\text{m}, -1.5\ \mu\text{m})\}$. A 30° convex arc connects the points $(-1\ \mu\text{m}, 1.5\ \mu\text{m})$ and $(-1\ \mu\text{m}, -1.5\ \mu\text{m})$. Therefore, the diameter and the width of the tip are 3 μm and 2 μm, respectively. (a) The density and contour plots of the magnetic field surrounding the magnetic tip. The arrows show the direction of the magnetic field. (b) Zoom-in plot of the magnetic field in the dashed white box in (a). (c) The component B_x along the dashed white line in (b). (d) The component B_x along the dashed green line in (b), 100 nm away from the top of the arc.

V. DISCUSSION AND CONCLUSION

Our scheme for squeezing and entangling an ensemble of electronic spins can be realized using a diamond nanowire [33–36]. We consider a single-crystal diamond nanowire (DNW) with a diameter of $d \sim 9.2$ nm and a length of $L \sim 1.45\ \mu$m [33]. The existing experimental technology can even make a thinner and lighter DNW to allow a stronger coupling [35,36]. The mass density of diamond is typically $\rho_m \sim 3000\ \text{kg/m}^3$. Thus the mass of the DNW is $\sim 2 \times 10^{-19}$ kg. The Young's modulus, E, of diamond can vary from ~40 to ~900 GPa [36,53]. We choose the typical value, $E = 300$ GPa, for our DNW yielding a resonance frequency of $\omega_m = 1.88^2 \frac{d}{L^2}\sqrt{\frac{E}{16\rho_m}} \approx 2\pi \times 6.1$ MHz for its fundamental mode. The zero-point fluctuation is correspondingly $x_{\text{zp}} \sim 2.2$ pm. The quality factor of the DNW can be over one million [33]. So, it is reasonable to take $Q_m = 10^6$. At a cryogenic temperature $T = 10$ mK, we have the thermal excitation of $\bar{n} = 33$.

We assume the distance of the closest NV centers along the axis of DNW to be 6nm corresponding to an energy shift of about $2\pi \times 0.3$ MHz due to the dipole-dipole interaction [54], which is negligible in comparison with the mechanical resonance frequency. The NV centers can be arranged as an array with precise position in an ultrathin film of diamond [55–57]. A large magnetic field gradient up to 4×10^7T/m has been reported in the magnetic disk drive system [58,59]. In magnetic resonance force microscopy systems, a gradient

larger than 10^6T/m has been realized [60–63]. The magnetic field gradient can be nearly constant over 100nm in depth [60]. Below we will apply a gradient about 2×10^5T/m or less.

Now we discuss the experimental implementation for the squeezed spin state and the creation of the GHZ state. We consider 20 spins embedded in the DNW over 120 nm along the axis. With choosing a magnetic gradient $G_B = 7.5 \times 10^4$ T m^{-1}, the optimal phase for squeezing, $\theta_{\rm opt} = 0.16$ rad, can be achieved at $t_m = 3 \times 10^3 T_m$ corresponding to $m\bar{n}/Q_m \approx 0.1$. The spins can be squeezed by 5.9 dB as a result. The GHZ state can only be generated at $\theta = \pi/2$. Such large geometric phase requires a large magnetic gradient and a large zero-point fluctuation. Using a magnetic gradient $G_B = 2.3 \times 10^5$T m^{-1}, we have $g_x/\omega_m \approx 0.0046$ ($g_x/2\pi \approx 28$ kHz) yielding $\theta_x(t_m) = \pi/2$ at $t_m = 3 \times 10^3 T_m$. As a minimum test, let us choose 4 spins implanted in the DNW requiring a length of at least 18 nm along the axis of the DNW; then we obtain a fidelity of $F = 0.62$. If we can create a uniform magnetic field B_x over ∼120 nm allowing us to embed 20 spins in the DNW, then we can generate the GHZ state with the same fidelity of $F = 0.62$ at $t_m = 3 \times 10^3 T_m$. It is noticeable, however, that the geometric phase protocol can only create the GHZ state for an even number of spins. On the other hand, if we are interested in squeezing and entangling a few spins, e.g., 4 spins, then the applied gradient can be 10^6 T/m order and the operation can be completely within a few cycles of mechanical vibration. As a result, the squeezing and the fidelity of the GHZ state can be larger.

The evolution period is $2\pi/\omega_m = 0.16$ μs for $\omega_m = 2\pi \times 6.1$ MHz. At t_m, the mechanical resonator is decoupled from the spins. So, we need read out the state of spins within time much smaller than 160 ns.

The large but detrimental Zeeman splitting of the ground states of spins caused by a large magnetic gradient limits the usable number of spins. In the discussion above, we neglect the inhomogeneous broadening of the coupling, g_x, caused by the fluctuation of the magnetic field in the transversal direction. It is reasonable only over tens of nm if $G_B = 10^6$ T/m is applied. Actually, the fluctuation of the magnetic field in the transversal direction will also reduce the fidelity of the target state. These factors limit the obtainable squeezing degree, the number of entangled spins, and the fidelity as well. By applying smaller gradient G_B, the area of uniform field increases. However, the coupling rate reduces. As a result, we need longer evolution time, which is in turn limited by the mechanical quality factor and the thermal excitation. Therefore, the generation of the SSS state and the GHZ state for $N > 20$ spins is quite challenging.

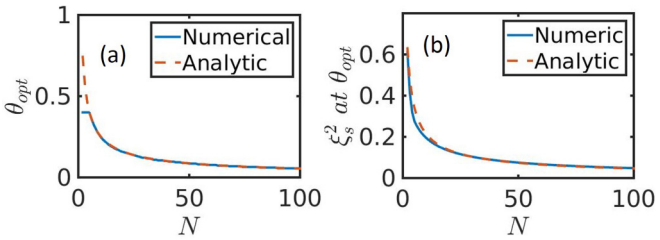

FIG. 7. Checking the optimal phase $\theta_{\rm opt}$ for achieving the maximal squeezing in the absence of mechanical decay. (a) The optimal phase $\theta_{\rm opt}$ for different spin number N. The dashed line is fitted by $\theta_{\rm opt} = 6^{-1/6} N^{-2/3}$. (b) The maximal squeezing at $\theta_{\rm opt}$ for different spin number N. The dashed line is fitted by $\xi_s^2 = N^{-2/3}$.

In summary, we couple up to 20 spins in nanodiamond to a nanomechanical resonator mediated by a magnetic field gradient. At cryogenic temperature, we show a squeezing of ∼5.9 dB and the generation of the GHZ state with a fidelity of $F \sim 0.62$ at the particular time when the mechanical motion decouples from the spins. Our scheme is based on the geometric phase control and therefore is robust against thermal noise, and many other types of noise.

ACKNOWLEDGMENTS

This research was supported in part by the ARC Centre of Excellence in Engineered Quantum Systems (EQuS), Project No. CE110001013, and in part by the National Natural Science Foundation of China (Grant No. 11204080).

APPENDIX : OPTIMAL PHASE FOR MAXIMAL SQUEEZING

We numerically study the optimal geometric phase and the corresponding maximal squeezing parameter ξ_s^2 as a function of number of spins. Rather than the formula $\theta_{\rm opt} = 24^{1/6}(N/2)^{-2/3}$ [64], we find the optimal phase in our case to be $\theta_{\rm opt} = 6^{-1/6}(N/2)^{-2/3}$ by fitting the numerical results; see Fig. 7.

[1] Gopalakrishnan Balasubramanian, Philipp Neumann, Daniel Twitchen, Matthew Markham, Roman Kolesov, Norikazu Mizuochi, Junichi Isoya, Jocelyn Achard, Johannes Beck, Julia Tissler, Vincent Jacques, Philip R. Hemmer, Fedor Jelezko, and Jörg Wrachtrup, Ultralong spin coherence time in isotopically engineered diamond, Nat. Mater. **8**, 383 (2009).

[2] P. L. Stanwix, L. M. Pham, J. R. Maze, D. Le Sage, T. K. Yeung, P. Cappellaro, P. R. Hemmer, A. Yacoby, M. D. Lukin, and R. L. Walsworth, Coherence of nitrogen-vacancy electronic spin ensembles in diamond, Phys. Rev. B **82**, 201201(R) (2010).

[3] Edited by Steven Prawer and Igor Aharonovich, *Quantum Information Processing with Diamond: Principles and Applications* (Woodhead Publishing, London, 2014).

[4] Lilian Childress and Ronald Hanson, Diamond NV centers for quantum computing and quantum networks, MRS Bull. **38**, 134 (2013).

[5] J. R. Weber, W. F. Koehl, J. B. Varley, A. Janotti, B. B. Buckley, C. G. Van de Walle, and D. D. Awschalom, Quantum computing with defects, Proc. Natl. Acad. Sci. U.S.A. **107**, 8513 (2010).

[6] Luozhou Li, Tim Schröder, Edward H. Chen, Michael Walsh, Igal Bayn, Jordan Goldstein, Ophir Gaathon, Matthew E. Trusheim, Ming Lu, Jacob Mower, Mircea Cotlet, Matthew L. Markham, Daniel J. Twitchen, and Dirk Englund, Coherent spin control of a nanocavity-enhanced qubit in diamond, Nat. Commun. **6**, 6173 (2015).

[7] Keyu Xia and Jason Twamley, Solid-state optical interconnect between distant superconducting quantum chips, Phys. Rev. A **91**, 042307 (2015).

[8] J. M. Taylor, P. Cappellaro, L. Childress, L. Jiang, D. Budker, P. R. Hemmer, A. Yacoby, R. Walsworth, and M. D. Lukin, High-sensitivity diamond magnetometer with nanoscale resolution, Nat. Phys. **4**, 810 (2008).

[9] Nan Zhao, Jian-Liang Hu, Sai-Wah Ho, Jones T. K. Wan, and R. B. Liu, Atomic-scale magnetometry of distant nuclear spin clusters via nitrogen-vacancy spin in diamond, Nat. Nanotechnol. **6**, 242 (2011).

[10] R. S. Said, D. W. Berry, and J. Twamley, Nanoscale magnetometry using a single-spin system in diamond, Phys. Rev. B **83**, 125410 (2011).

[11] Thomas Wolf, Philipp Neumann, Kazuo Nakamura, Hitoshi Sumiya, Takeshi Ohshima, Junichi Isoya, and Jörg Wrachtrup, Subpicotesla Diamond Magnetometry, Phys. Rev. X **5**, 041001 (2015).

[12] D. Sheng, S. Li, N. Dural, and M. V. Romalis, Subfemtotesla Scalar Atomic Magnetometry Using Multipass Cells, Phys. Rev. Lett. **110**, 160802 (2013).

[13] Keyu Xia, Nan Zhao, and Jason Twamley, Detection of a weak magnetic field via cavity-enhanced Faraday rotation, Phys. Rev. A **92**, 043409 (2015).

[14] Hannah Clevenson, Matthew E. Trusheim, Carson Teale, Tim Schröder, Danielle Braje, and Dirk Englund, Broadband magnetometry and temperature sensing with a light-trapping diamond waveguide, Nat. Phys. **11**, 393 (2015).

[15] P. Neumann, I. Jakobi, F. Dolde, C. Burk, R. Reuter, G. Waldherr, J. Honert, T. Wolf, A. Brunner, J. H. Shim, D. Suter, H. Sumiya, J. Isoya, and J. Wrachtrup, High-precision nanoscale temperature sensing using single defects in diamond, Nano Lett. **13**, 2738 (2013).

[16] Junfeng Wang, Fupan Feng, Jian Zhang, Jihong Chen, Zhongcheng Zheng, Liping Guo, Wenlong Zhang, Xuerui Song, Guoping Guo, Lele Fan, Chongwen Zou, Liren Lou, Wei Zhu, and Guanzhong Wang, High-sensitivity temperature sensing using an implanted single nitrogen-vacancy center array in diamond, Phys. Rev. B **91**, 155404 (2015).

[17] Abdelghani Laraoui, Halley Aycock-Rizzo, Yang Gao, Xi Lu, Elisa Riedo, and Carlos A. Meriles, Imaging thermal conductivity with nanoscale resolution using a scanning spin probe, Nat. Commun. **6**, 8954 (2015).

[18] Kyu Young Han, Katrin I. Willig, Eva Rittweger, Fedor Jelezko, Christian Eggeling, and Stefan W. Hell, Three-dimensional stimulated emission depletion microscopy of nitrogen-vacancy centers in diamond using continuous-wave light, Nano Lett. **9**, 3323 (2009).

[19] Jian Ma, Xiaoguang Wang, C. P. Sun, and Franco Nori, Quantum spin squeezing, Phys. Rep. **509**, 89 (2011).

[20] C. D. Hamley, C. S. Gerving, T. M. Hoang, E. M. Bookjans, and M. S. Chapman, Spin-nematic squeezed vacuum in a quantum gas, Nat. Phys. **8**, 305 (2012).

[21] Onur Hosten, Nils J. Engelsen, Rajiv Krishnakumar, and Mark A. Kasevich, Measurement noise 100 times lower than the quantum-projection limit using entangled atoms, Nature (London) **529**, 505 (2016).

[22] Emanuele G. Dalla Torre, Johannes Otterbach, Eugene Demler, Vladan Vuletic, and Mikhail D. Lukin, Dissipative Preparation of Spin Squeezed Atomic Ensembles in a Steady State, Phys. Rev. Lett. **110**, 120402 (2013).

[23] T. Fernholz, H. Krauter, K. Jensen, J. F. Sherson, A. S. Sørensen, and E. S. Polzik, Spin Squeezing of Atomic Ensembles via Nuclear-Electronic Spin Entanglement, Phys. Rev. Lett. **101**, 073601 (2008).

[24] S. D. Bennett, N. Y. Yao, J. Otterbach, P. Zoller, P. Rabl, and M. D. Lukin, Phonon-Induced Spin-Spin Interactions in Diamond Nanostructures: Application to Spin Squeezing, Phys. Rev. Lett. **110**, 156402 (2013).

[25] Christopher Eltschka and Jens Siewert, Entanglement of Three-Qubit Greenberger-Horne-Zeilinger Symmetric States, Phys. Rev. Lett. **108**, 020502 (2012).

[26] D. D. Bhaktavatsala Rao, Sen Yang, and Jörg Wrachtrup, Generation of entangled photon strings using NV centers in diamond, Phys. Rev. B **92**, 081301 (2015).

[27] Jonathan A. Jones, Steven D. Karlen, Joseph Fitzsimons, Arzhang Ardavan, Simon C. Benjamin, G. Andrew D. Briggs, and John J. L. Morton, Magnetic field sensing beyond the standard quantum limit using 10-spin noon states, Science **324**, 1166 (2009).

[28] Yan-Lei Zhang, Chang-Ling Zou, Xu-Bo Zou, Liang Jiang, and Guang-Can Guo, Phonon-induced spin squeezing based on geometric phase, Phys. Rev. A **92**, 013825 (2015).

[29] Y. Tao, J. M. Boss, B. A. Moores, and C. L. Degen, Single-crystal diamond nanomechanical resonators with quality factors exceeding one million, Nat. Commun. **5**, 3638 (2014).

[30] Yonhua Tzeng, Yu-Chun Chen, An-Jen Cheng, Ying-Ting Hung, Chen-Sheng Yeh, Minseo Par, and Bogdan M. Wilamowski, Chemically vapor deposited diamond-tipped one-dimensional nanostructures and nanodiamond-silica-nanotube composites, Diam. Relat. Mater. **18**, 173 (2009).

[31] Thai M. Hong, Jonghoon Ahn, Jaehoon Bang, and Tongcang Li, Electron spin control of optically levitated nanodiamonds in vacuum, Nat. Commun. **7**, 12250 (2016).

[32] D. E. Chang, C. A. Regal, S. B. Papp, D. J. Wilson, J. Ye, O. Painter, H. J. Kimble, and P. Zoller, Cavity opto-mechanics using an optically levitated nanosphere, Proc. Natl. Acad. Sci. U.S.A. **107**, 1005 (2010).

[33] Y. Tao and C. L. Degen, Single-crystal diamond nanowire tips for ultrasensitive force microscopy, Nano Lett. **15**, 7893 (2015).

[34] C. H. Hsu and J. Xu, Diamond nanowire—a challenge from extremes, Nanoscale **4**, 5293 (2012).

[35] Thomas C. Fitzgibbons, Malcolm Guthrie, En shi Xu, Vincent H. Crespi, Stephen K. Davidowski, George D. Cody, Nasim Alem, and John V. Badding, Benzene-derived carbon nanothreads, Nat. Mater. **14**, 43 (2015).

[36] Haifei Zhan, Gang Zhang, Vincent B. C. Tan, Yuan Cheng, John M. Bell, Yong-Wei Zhang, and Yuantong Gu, From brittle to ductile: A structure dependent ductility of diamond nanothread, Nanoscale **8**, 11177 (2016).

[37] F. Dolde, H. Fedder, M. W. Doherty, T. Nöbauer, F. Rempp, G. Balasubramanian, T. Wolf, F. Reinhard, L. C. L. Hollenberg, F. Jelezko, and J. Wrachtrup, Electric-field sensing using single diamond spins, Nat. Phys. **7**, 459 (2011).

[38] J. Teissier, A. Barfuss, P. Appel, E. Neu, and P. Maletinsky, Strain Coupling of a Nitrogen-Vacancy Center Spin to a Diamond Mechanical Oscillator, Phys. Rev. Lett. **113**, 020503 (2014).

[39] M. W. Doherty, F. Dolde, H. Fedder, F. Jelezko, J. Wrachtrup, N. B. Manson, and L. C. L. Hollenberg, Theory of the ground-state spin of the NV^- center in diamond, Phys. Rev. B **85**, 205203 (2012).

[40] S. Felton, A. M. Edmonds, M. E. Newton, P. M. Martineau, D. Fisher, D. J. Twitchen, and J. M. Baker, Hyperfine interaction in the ground state of the negatively charged nitrogen vacancy center in diamond, Phys. Rev. B **79**, 075203 (2009).

[41] Q. Chen, I. Schwarz, F. Jelezko, A. Retzker, and M. B. Plenio, Optical hyperpolarization of ^{13}C nuclear spins in nanodiamond ensembles, Phys. Rev. B **92**, 184420 (2015).

[42] Ran Fischer, Andrey Jarmola, Pauli Kehayias, and Dmitry Budker, Optical polarization of nuclear ensembles in diamond, Phys. Rev. B **87**, 125207 (2013).

[43] Benjamin Smeltzer, Lilian Childress, and Adam Gali, ^{13}c hyperfine interactions in the nitrogen-vacancy center in diamond, New J. Phys. **13**, 025021 (2011).

[44] T. Holstein and H. Primakoff, Field dependence of the intrinsic domain magnetization of a ferromagnet, Phys. Rev. **58**, 1098 (1940).

[45] D. Nagy, G. Kónya, G. Szirmai, and P. Domokos, Dicke-Model Phase Transition in the Quantum Motion of a Bose-Einstein Condensate in an Optical Cavity, Phys. Rev. Lett. **104**, 130401 (2010).

[46] W. Magnus, On the exponential solution of differential equations for a linear operator, Commun. Pure Appl. Math. **7**, 649 (1954).

[47] A. Carollo, I. Fuentes-Guridi, M. França Santos, and V. Vedral, Geometric Phase in Open Systems, Phys. Rev. Lett. **90**, 160402 (2003).

[48] Shi-Liang Zhu, Z. D. Wang, and Paolo Zanardi, Geometric Quantum Computation and Multiqubit Entanglement with Superconducting Qubits inside a Cavity, Phys. Rev. Lett. **94**, 100502 (2005).

[49] Zheng-Yuan Xue and Z. D. Wang, Simple unconventional geometric scenario of one-way quantum computation with superconducting qubits inside a cavity, Phys. Rev. A **75**, 064303 (2007).

[50] A. Jarmola, V. M. Acosta, K. Jensen, S. Chemerisov, and D. Budker, Temperature- and Magnetic-Field-Dependent Longitudinal Spin Relaxation in Nitrogen-Vacancy Ensembles in Diamond, Phys. Rev. Lett. **108**, 197601 (2012).

[51] P. Rabl, S. J. Kolkowitz, F. H. L. Koppens, J. G. E. Harris, P. Zoller, and M. D. Lukin, A quantum spin transducer based on nanoelectromechanical resonator arrays, Nat. Phys. **6**, 602 (2010).

[52] Zhang-qi Yin, Tongcang Li, Xiang Zhang, and L. M. Duan, Large quantum superpositions of a levitated nanodiamond through spin-optomechanical coupling, Phys. Rev. A **88**, 033614 (2013).

[53] J. Xue, Z. Jijun, and J. Xin, Mechanical and electronic properties of diamond nanowires under tensile strain from first principles, Nanotechnology **22**, 405705 (2011).

[54] J. R. Maze, A. Gali, E. Togan, Y. Chu, A. Trifonov, E. Kaxiras, and M. D. Lukin, Properties of nitrogen-vacancy centers in diamond: The group theoretic approach, New J. Phys. **13**, 025025 (2011).

[55] S. Ali Momenzadeh, Rainer J. Stöhr, Felipe Favaro de Oliveira, Andreas Brunner, Andrej Denisenko, Sen Yang, Friedemann Reinhard, and Jörg Wrachtrup, Nanoengineered diamond waveguide as a robust bright platform for nanomagnetometry using shallow nitrogen vacancy centers, Nano Lett. **15**, 165 (2015).

[56] Jianming Cai, Alex Retzker, Fedor Jelezko, and Martin B. Plenio, A large-scale quantum simulator on a diamond surface at room temperature, Nat. Phys. **9**, 168 (2013).

[57] A. A. Zyuzin, M. D. Hook, and A. A. Burkov, Parallel magnetic field driven quantum phase transition in a thin topological insulator film, Phys. Rev. B **83**, 245428 (2011).

[58] C. Tsang, C. Bonhote, Q. Dai, H. Do, B. Knigge, Y. Ikeda, Q. Le, B. Lengsfield, J. Lille, J. Li, S. MacDonald, A. Moser, V. Nayak, R. Payne, N. Robertson, M. Schabes, N. Smith, K. Takano, P. van der Heijden, W. Weresin, M. Williams, and M. Xiao, Head challenges for perpendicular recording at high areal density, IEEE Trans. Magn. **42**, 145 (2006).

[59] Y. Tao, A. Eichler, T. Holzherr, and C. L. Degen, Ultrasensitive mechanical detection of magnetic moment using a commercial disk drive write head, Nat. Commun. **7**, 12714 (2016).

[60] H. J. Mamin, M. Poggio, C. L. Degen, and D. Rugar, Nuclear magnetic resonance imaging with 90-nm resolution, Nat. Nanotechnol. **2**, 301 (2007).

[61] Jonilyn G. Longenecker, H. J. Mamin, Alexander W. Senko, Lei Chen, Charles T. Rettner, Daniel Rugar, and John A. Marohn, High-gradient nanomagnets on cantilevers for sensitive detection of nuclear magnetic resonance, ACS Nano **6**, 9637 (2012).

[62] H. J. Mamin, C. T. Rettner, M. H. Sherwood, L. Gao, and D. Rugar, High field-gradient dysprosium tips for magnetic resonance force microscopy, Appl. Phys. Lett. **100**, 013102 (2012).

[63] C. L. Degen, M. Poggio, H. J. Mamin, C. T. Rettner, and D. Rugar, Nanoscale magnetic resonance imaging, Proc. Natl. Acad. Sci. U.S.A. **106**, 1313 (2009).

[64] Masahiro Kitagawa and Masahito Ueda, Squeezed spin states, Phys. Rev. A **47**, 5138 (1993).